ISBN: 978-3-95450-179-3 doi:10.18429/JACoW-FEL2017-WEP061

THERMAL STRESS ANALYSIS OF A THIN DIAMOND CRYSTAL UNDER REPEATED FREE ELECTRON LASER HEAT LOAD*

Bo Yang†, Department of Mechanical and Aerospace Engineering,
University of Texas at Arlington, Arlington, TX 76019, USA
Juhao Wu‡, SLAC National Accelerator Laboratory, Menlo Park, California, 94025, USA

Abstract

Thin crystals are used as many important optical elements in XFELs, such as monochromators and spectrometers. To function properly, they must survive the ever-increasing heat load under repeated pulses. Here, we conduct a thermal stress analysis to examine the crystal lattice distortion due to the thermal load under various rep rates from 0.1 to 1 MHz. The thermal field is obtained by solving the transient heat transfer equations. The temperature-dependent material properties are used. It is shown that for pulse adsorption energy around tens of μJ over a spot size of 10 μm, the thermal response of diamond is sensitive to rep rate. The thermal strain components are very different in the in- and out-of-plane directions, due to different constraint conditions. It suggests complicated strain effects in the Bragg and Laue diffraction cases.

INTRODUCTION

XFELs generate high peak-power pulses with atomic and femtosecond scale resolution, impacting high-frontier scientific research [1,2]. Thin crystals are used in several important elements, such as monochromators [3,4], single-shot spectrometers [5–7], and other applications [8]. In pursuit of high-brightness XFELs, the power has been increased by orders of magnitude, so the thin crystals will experience much increased heat load. Thus, it is important to understand their photo-thermo-mechanical behaviours at higher temperature. Here, we perform a thermal stress analysis to elucidate the deformation field in a thin diamond crystal subjected to repeated heat load of XFEL pulses. The stress/strain field is obtained with a thermal field as a loading source by solving the static equilibrium equation. The thermal field is modelled by solving transient heat transfer equations and material properties, such as the thermal expansion, heat capacity [9] and thermal conductivity [10] valid up to temperatures ~3000 K. The problem is solved with a finite volume method [11,12]. The case of a 40-μm thick plate with a Gaussian beam of FWHM of 20 μm is studied with rep rates from 0.1 to 1 MHz. For a pulse depositing tens of μJ energy, the temperature that a next pulse sees ratchets up slowly at 0.1-0.2 MHz, but upsurges at higher rep rates. At 1 MHz, a runaway increase of temperature is found after a few pulses. It is because the heat relaxation rate through conduction decreases with temperature due to decreasing heat conductivity. The thermal stress/strain fields are analysed with a residual thermal field as a loading source. The strain components are different, implying complicated strain effects in Bragg and Laue diffractions.

*Work supported by the US Department of Energy (DOE) under contract DE-AC02-76SF00515 and the US DOE Office of Science Early Career Research Program grant FWP-2013-SLAC-100164.
†boyang@uta.edu
‡jhwu@slac.stanford.edu

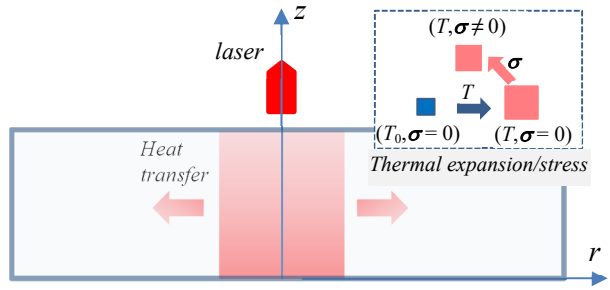

Figure 1: Schematics of instantaneous heating and subsequent heat transfer upon laser energy deposition in a thin crystal. The inset on the upper-right shows the thermal expansion and the stress to be built up due to constraint. The cylindrical coordinate with axisymmetry is used.

PROBLEM FORMULATION

Governing Equations

An XFEL impinging on a crystal would interact with the electrons and deposit a part of energy first onto the electrons [13]. Later the energy is transferred to the lattice raising the temperature. This process occurs at the pico-to-nano second scale. Then, the thermalized lattice expands emitting stress waves at the nano-to-tens-of-nano second scale at the sound speed [14]. The thermal diffusion will start, but not become effective until hundreds of nanoseconds. During this time, the stress waves would have bounced back and forth between boundaries for tens of times. If passive damping is instated, the inertia effect will soon become trivial. Thus, we assume that the specimen is in the mechanical equilibrium despite the transient heat transfer. The thermal field will significantly affect the deformation field, but the effect of deformation on thermal field is trivial. We analyse the processes of transient heat transfer and resulting thermal stress field. A cylindrical coordinate system (r, θ, z) is used with z-axis normal to the crystal surface as in Fig. 1. Only a pulse perpendicular to the crystal surface is studied.

The equilibrium equation without body forces is:

$$\nabla \cdot \boldsymbol{\sigma} = 0\,, \tag{1}$$

where $\boldsymbol{\sigma}$ is the stress tensor. Assuming the isotropic thermoelasticity, the constitutive law is given by [15]:

ISBN: 978-3-95450-179-3 doi:10.18429/JACoW-FEL2017-WEP061

$$\boldsymbol{\sigma} = 2G\left(\boldsymbol{\varepsilon} - \frac{1}{3}\mathrm{tr}(\boldsymbol{\varepsilon})\boldsymbol{I}\right) + 3K_b\left(\frac{1}{3}\mathrm{tr}(\boldsymbol{\varepsilon}) - \varepsilon_T\right)\boldsymbol{I}\,, \quad (2)$$

where G is the modulus of rigidity, K_b the bulk modulus, $\boldsymbol{\varepsilon}$ the strain tensor, ε_T the thermal strain, $\boldsymbol{I}$ the identity matrix, and $\mathrm{tr}(\boldsymbol{\varepsilon})$ the trace of $\boldsymbol{\varepsilon}$.

The equation of energy conservation is given by

$$\frac{dU_T}{dt} = -\nabla\cdot(-\kappa\nabla T)\,, \quad (3)$$

where T is the temperature, $U_T(=\int \rho C_v dT)$ the thermal energy density, κ the thermal conductivity, ρ the mass density, and C_v the specific heat.

The initial temperature is $T_0 = 300K$. The FEL pulse energy is partially absorbed raising the temperature. The FEL pulse is assumed to be Gaussian. It impinges perpendicularly to the crystal surface, assumed so that the problem can be reduced to be axisymmetric. The change of thermal energy density as a function of r and z is

$$\Delta U_T(r,z) = \frac{2I_0}{\pi a^2 L} e^{-\frac{2r^2}{a^2}} e^{-\frac{z}{L}}\,, \quad (3)$$

where I_0 is the FEL pulse energy, a the transverse FWHM of the Gaussian beam in the radial direction, and L the attenuation length. The temperature increase is determined from the relationship of U_T to T. The thermal insulation and traction-free boundary conditions are applied.

Material Properties

The thermal strain and specific heat capacity of diamond are taken from Ref.[9]. The thermal strain is given by

$$\varepsilon_T = \sum_{i=1}^{3} \frac{X_i\theta_i}{\exp\left(\frac{\theta_i}{T}\right)-1}\,, \quad (4)$$

where θ_i and X_i are constants, given by $\theta_1 = 200$ K, $\theta_2 = 880$ K, $\theta_3 = 2137.5$ K, $X_1 = 0.4369\times10^{-7}\mathrm{K}^{-1}$, $X_2 = 15.7867\times10^{-7}\mathrm{K}^{-1}$, $X_3 = 42.5598\times10^{-7}\mathrm{K}^{-1}$. The linear thermal expansion coefficient is $\alpha_T = \partial\varepsilon_T/\partial T$. The U_T is obtained through $\int \rho C_v dT$ with tabulated values of C_v up to T = 3000 K. The thermal conductivity is $\kappa = 2200$ $\mathrm{Wm^{-1}K^{-1}}$ for diamond at 300 K. Yet, it decreases rapidly with increasing temperature, to be 100 $\mathrm{Wm^{-1}K^{-1}}$ at T = 2000 K. The data of Ref. 10 from 300 K to 2000 K are averaged and fit to a power law: $\kappa = 23.9\times10^6\,T^{-1.63}$. Other materials constants are given as density $\rho = 3.51$ g/cm^3, shear modulus G = 508 GPa, and bulk modulus $K_b = 678$ GPa.

RESULTS AND DISCUSSION

Simulations were carried out at four rep rates: 0.1, 0.2, 0.5, and 1 MHz. The FWHM of the Gaussian beam is a = 20 μm. The pulse energy I_0 = 100 μJ. The attenuation length L = 50 μm, corresponding to ~4 keV X-ray. The crystal plate thickness h = 40 μm. In this case, the laser energy is about 55 % absorbed by the crystal. As the laser energy decreases, it raises the internal energy at the front (entry) surface about 2.2 times that at the back (exit) surface. This amount of energy is added to the system each pulse according to the rep rates. Eleven equal divisions are used to discretize the domain in the thickness direction. An adaptive mesh is used in the radial direction, with 10 equal divisions in near 10 μm distance, and 200 unequal divisions with increasing size outwards by gradient 1.015 in following 1490 μm distance, from the center. The time step is 10 ns. For each repetition rate, the simulation was run longer than 0.1 ms. Selected results are presented in Figs. 2–6. Figures 2(a)–(d) show the temperature evolution on the front surface (z = 0) at three radial distances r = 0, 20, 50 μm for the four rep rates. Figures 3(a)–(d) show the temperature profiles along the radial direction on the front surface for the four cases. Figures 4(a)–(d) show the corresponding three normal strain components, ε_r, ε_θ, and ε_z. Figures 5(a)–(d) and 6(a)–(d) show the same profiles as in Figs. 3 and 4, but on the middle plane of the layer. Based on the above results, some observations are made and discussed as follows.

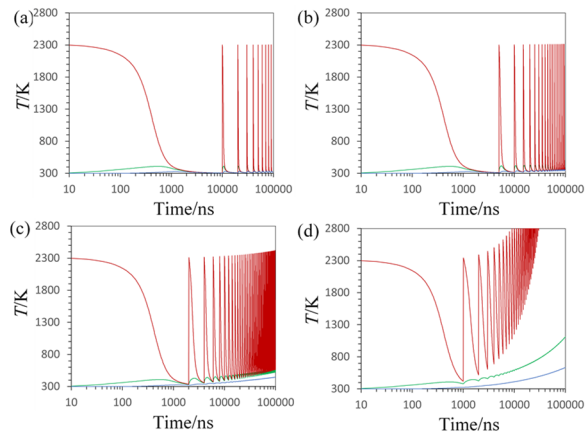

Figure 2: Temperature evolution at three radial distance r = 0 (red), 20 (green), 50 (blue) μm on the surface (z = 0) under repetition rates: (a) 0.1; (b) 0.2; (c) 0.5; (d) 1 MHz.

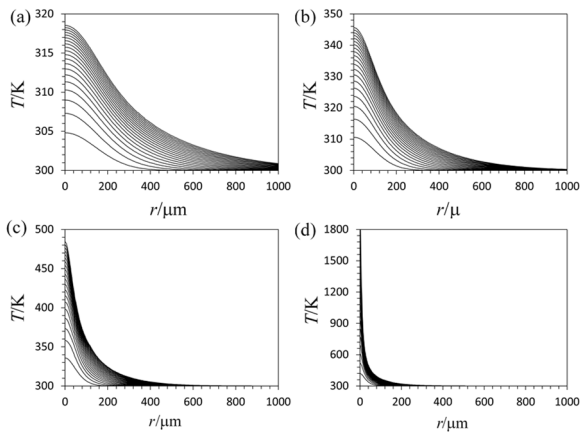

Figure 3. Temperature profiles along the radial axis at the front surface (z = 0) at times before a next pulse strikes under repetition rate: (a) 0.1; (b) 0.2; (c) 0.5; (d) 1 MHz. Twenty pulses are plotted in each case.

ISBN: 978-3-95450-179-3 doi:10.18429/JACoW-FEL2017-WEP061

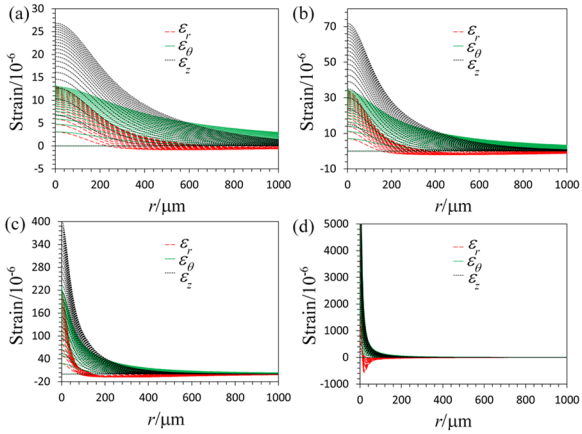

Figure 4. Profiles of strain components ε_r (red), ε_θ (green) and ε_z (black) along the radial axis at the front surface (z = 0) at times before a next pulse strikes under repetition rate: (a) 0.1; (b) 0.2; (c) 0.5; (d) 1 MHz. Twenty pulses are plotted in each case.

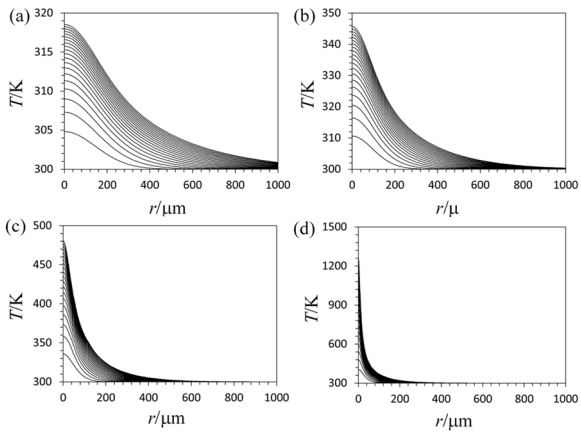

Figure 5. Temperature profiles along the radial axis at the middle plane (z = 20 μm) at times before a next pulse strikes under repetition rate: (a) 0.1; (b) 0.2; (c) 0.5; (d) 1 MHz. Twenty pulses are plotted in each case.

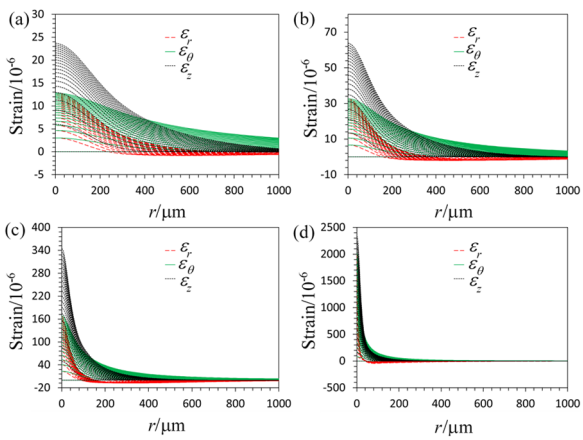

Figure 6. Profiles of strain components ε_r (red), ε_θ (green) and ε_z (black) along the radial axis at the middle plane (z = 20 μm) at times before a next pulse strikes under repetition rate: (a) 0.1; (b) 0.2; (c) 0.5; (d) 1 MHz. Twenty pulses are plotted in each case.

It may be seen from Figs. 2, 3, and 5 that the thermal response of diamond is sensitive to repetition rate when it gets near 1 MHz at the energy deposition of tens of μJ per pulse over a spot size around 10 μm. At 100 – 200 kHz, the temperature increases with each pulse, but slowly. At 500 kHz, the temperature ratchets up much more quickly. At 1 MHz, a runaway of temperature is observed only after a few pulses. At 100 – 200 kHz, the temperature is nearly uniform across thickness upon relaxation after each pulse and before the next pulse. In contrast, at the higher rep rates, the temperature rises so high and the thermal diffusivity drops so significantly that the thermal equilibrium cannot be established across the thickness between pulses. At 1 MHz, the runaway thermal spike occurs near the front surface where the laser beams strike. At low temperatures, the strain resulting from thermal expansion is proportional to the temperature change with a coefficient about 1 x 10^{-6} K^{-1}, indicating that diamond is an excellent material against thermal expansion. At higher temperatures, its strong lattice force constants soften, leading to much increased linear thermal expansion coefficient. It quickly reaches 4 x 10^{-6} K^{-1} at ~1000 K and keeps rising though at a slower rate, similarly to how its specific heat varies with temperature. The spatial variation of strain follows that of temperature as in these figures. The strain fields are also somewhat different at the surface and inside the layer due to three-dimensional effect across the thickness and along the radial direction.

Due to the different constraint conditions, the strain components ε_r, ε_θ, and ε_z turn out to be very different. ε_r and ε_θ are equal to each other along the center line ($r = 0$) of the FEL spot, as in Figs. 4 and 6. This is consistent with the corresponding analytical result demonstrating the validity of the present numerical solution. Importantly, it is seen that ε_z is nearly twice the other two normal components. Since the Bragg and Laue cases of diffraction use reflection planes ranging from parallel to the surface to tilted by a large angle from the surface, it becomes complicated how the strain field affects them. It necessitates a detailed thermomechanical study to understand the thermal effect on diffraction. The present study and alike provide the 3-D strain field in a thin crystal under heat load. The relationship of thin-crystal-based optical element sensitivity to strain is yet to be established.

SUMMARY

Transient heat transfer and static thermal stress analyses are performed for a thin diamond crystal under repeated FEL heat load. The formulation is phenomenological. The problem is solved with a finite volume method [14,16]. The realistic material properties of diamond from room temperature to elevated temperature are used. The range of rep rates from 0.1 to 1 MHz is considered. For deposition energy of tens of μJ per pulse over a spot size of 10 μm, the thermal response of diamond is found

ISBN: 978-3-95450-179-3 doi:10.18429/JACoW-FEL2017-WEP061

to be quite sensitive to the repetition rate. The instantaneous maximum temperature due to a single pulse can reach over 2000 K. It relaxes to a certain extent before a next pulse. The temperature and hence the thermal strain field ratchet up with pulses, slowly at 0.1–0.2 MHz, but much accelerated at 0.5 MHz and above. At 1 MHz, a runaway increase of temperature is observed after only a few pulses. Meanwhile the temperature increases, the thermal conductivity drops. It slows down the thermal relaxation in the radial direction and across the thickness. Finally, it is shown that the strain components are very different in the in- and out-of-plane directions. It implies complicated strain effect in the Bragg and Laue diffractions. The present analysis and alike using realistic material properties are necessary to understand the limits to using diamond in the optical elements for XFEL's under high rep rate.

REFERENCES

[1] Emma, P. *et al.,* "First lasing and operation of an ångstrom-wavelength free-electron laser." *Nature Photonics* **4**, 641–647 (2010).

[2] Ishikawa, T. *et al.,* "A compact X-ray free-electron laser emitting in the sub-angstrom region." *Nature Photonics* **6**, 540–544 (2012).

[3] Geloni, G., Kocharyan, V. and Saldin, E., "A novel self-seeding scheme for hard X-ray FELs." *Journal of Modern Optics* **58**, 1391–1403 (2011).

[4] Amann, J. *et al.,* "Demonstration of self-seeding in a hard-X-ray free-electron laser." *Nature Photonics* **6**, 693–698 (2012).

[5] Yabashi, M. *et al.,* "Single-shot spectrometry for X-ray free-electron lasers." *Physical Review Letters* **97**, 084802 (2006).

[6] Zhu, D. *et al.,* "A single-shot transmissive spectrometer for hard x-ray free electron lasers." *Applied Physics Letters* **101**, 034103 (2012).

[7] Rehanek, J. *et al.,* "The hard X-ray photon single-shot spectrometer of SwissFEL—initial characterization." *Journal of Instrumentation* **12**, A07001 (2017).

[8] Shvyd'ko, Y., Blank, V. and Terentyev, S., "Diamond x-ray optics: transparent, resilient, high-resolution, and wavefront preserving." *MRS Bulletin* **42**, 437–444 (2017).

[9] Reeber, R. R. and Wang, K., "Thermal expansion, molar volume and specific heat of diamond from 0 to 3000K." *Journal of Electronic Materials* **25**, 63–67 (1996).

[10] Wei, L., Kuo, P., Thomas, R., Anthony, T. and Banholzer, W., "Thermal conductivity of isotopically modified single crystal diamond." *Physical Review Letters* **70**, 3764 (1993).

[11] LeVeque, R. J., "Finite volume methods for hyperbolic problems." vol. 31, Cambridge University Press, 2002.

[12] Versteeg, H. K. and Malalasekera, W., "An introduction to computational fluid dynamics: the finite volume method." Pearson Education, 2007.

[13] Von der Linde, D., Sokolowski-Tinten, K. and Bialkowski, J., "Laser–solid interaction in the femtosecond time regime." *Applied Surface Science* **109**, 1–10 (1997).

[14] Yang, B., Wang, S. and Wu, J., "Transient thermal stress wave and vibrational analyses of a thin diamond crystal for X-ray FELs under high-repetition-rate operation." *Journal of Synchrotron Radiation* (under review).

[15] Shorr, B. F., "Thermal integrity in mechanics and engineering." Springer, 2015.

[16] Yang, B., Wu, J., Raubenheimer, T. O. and Feng, Y., "Fluid dynamics analysis of a gas attenuator for X-ray FELs under high-repetition-rate operation." *Journal of Synchrotron Radiation* **24** (2017).